Neural, Parallel, and Scientific Computations 22 (2014) 315-330

A MACROSCOPIC MODEL FOR PEDESTRIAN FLOW: COMPARISONS WITH EXPERIMENTAL RESULTS OF PEDESTRIAN FLOW IN CORRIDORS AND T-JUNCTIONS

R. ETIKYALA[1], S. GÖTTLICH[2], A. KLAR[1], AND S. TIWARI[1]

[1]Department of Mathematics, University of Kaiserslautern,
P.O. Box 3049, 67653 Kaiserslautern, Germany.
[2]Department of Mathematics, University of Mannheim,
A5, 6, 68131 Mannheim, Germany.
Corresponding author: Sudarsan Tiwari (tiwari@mathematik.uni-kl.de)

ABSTRACT. We present a macroscopic model for the flow of pedestrians including an optimal route choice. The optimal path of pedestrians is determined by solving the nonlinear Eikonal equation with a density-dependent speed function to minimize travel times and avoid high density areas. We use a finite pointset method to solve the governing equations and the Eikonal equation as well. We numerically study the pedestrian flow in straight corridors and T-junctions and compare our results with experimental data.

AMS (MOS) Subject Classification. 90B20, 35L60, 35L65.

1. Introduction

In recent years, research on pedestrian and traffic flow has become more popular and attracted to the interest of an increasing number of scientists. Analytical and numerical methods are effective tools to investigate, predict and simulate the complex behavior of pedestrians. A description of human crowds is strongly non-standard due to the intelligence and decision making abilities of pedestrians. Their behavior depends on the physical form of individuals and on the purpose and conditions of their motion. Numerous models for pedestrian flow have been proposed on different description levels. On the microscopic (individual based) level, models relying on Newtons equations have been developed as well as vision-based models or cellular automata models, see Refs. [14, 15] and [2, 8, 24, 27] for further references. Equations on the mesoscopic or kinetic level are discussed for example in Refs. [9, 13]. Hydrodynamic pedestrian flow equations involving equations for the density and mean velocity of the flow are derived in Refs. [3, 13]. The first modeling attempt is due to Hughes [16] who defined the crowd as a 'thinking fluid' and described the time

Received December 31, 2013

evolution of its density using a scalar conservation law. For a general recent review on pedestrian flow models we refer again to Refs. [2, 8].

The only available results using the Hughes' model for simulations of pedestrian flows on a large platform with a rectangular or circular obstacle in its interior can be found in [18, 23]. To the best of our knowledge, none of the works analyzed bi-directional pedestrian flow in straight corridors and T-junctions using Hughes' approach. However, the pedestrian flow in straight corridors and T-junctions is an important issue, for instance for the evacuation of buildings. In this kind of structure, lane formation, bottleneck situations, merging or split flow are possible scenarios that should be captured.

In this paper, we analyze the pedestrian flow in corridors and through T-junctions using the macroscopic model derived in [10]. For our numerical study, we consider the experiments recently conducted by J. Zhang et al. [32, 33, 34], in which they develop fundamental diagrams in straight corridors and T-junctions. To do so, we present a macroscopic model using Hughes approach and compare our results with experimental data. We use a finite pointset method to solve the governing equations. To solve the Eikonal equation, we apply a least square approximation coupled to the idea of fast marching [28]. Note that our method differs in approximating the derivatives of the Eikonal equation and can be used on arbitrary grids and complex geometries.

The paper is organized in the following way: In Section 2 the mathematical model is presented. Section 3 contains the numerical method to solve the governing equations. Section 4 is devoted to the numerical results and a comparison with experimental data. Finally, Section 5 concludes the present work.

2. Mathematical Model

We consider the mathematical model for pedestrian flow [10] including an optimal path computation as proposed by Hughes. Denoting by ρ the density of pedestrians and by u their mean velocity, the model is described by the following mass and momentum balance equations

$$\begin{aligned} \partial_t \rho + \nabla_x \cdot (\rho u) &= 0 \\ \partial_t u + (u \cdot \nabla_x) u &= G(x, u, \rho) + \hat{F}(\rho, u), \end{aligned} \tag{2.1}$$

where $G(x, u, \rho)$ is the relaxation force towards the desired direction and velocity given by

$$G(x, u, \rho) = \frac{1}{T}(U(\rho(x))d - u). \tag{2.2}$$

Here T denotes the reaction time describing how fast pedestrian can correct their current velocity to the desired one. The function $U(\rho)$ describes the speed-density relationship and d is the unit vector in the direction of the optimal path. There are many speed-density relationships available [20]. For our simulations, we choose

$$U(\rho(x)) = u_{max}\Big(1 - \Big(\frac{\rho}{\rho_{max}}\Big)^{n_1}\Big)^{n_2}, \tag{2.3}$$

for some real values n_1 and n_2, the maximum velocity u_{max} and the maximum density ρ_{max}. The interaction force $\hat{F}$ is given by

$$\hat{F}(\rho, u) = \int F(x - y, u(x) - u(y))\rho(y)dy \tag{2.4}$$

with

$$F(x, v) = F_{int}(x) + F_{diss}(x, v).$$

The interaction force F_{int} is given by

$$F_{int} = F_{int}(x) = -\nabla_x V(\|x\|)$$

where V is an interaction potential of the form

$$V = V(x) = k_n \left(2R^2 - \|x\|(2R - \frac{\|x\|}{2})\right) H(2R - \|x\|)$$

and H is the Heaviside function. This yields

$$F_{int}(x) = k_n n(x)(2R - \|x\|)H(2R - \|x\|)$$

where

$$n = n(x) = \frac{x}{\|x\|}$$

is the normal unit vector. This force is complemented by a dissipative force, compare e.g. Ref. [14]. The dissipative force is given by

$$F_{diss} = \left(F^n_{diss} + F^t_{diss}\right) H(2R - \|x\|).$$

Here, the normal dissipative force is given by

$$F^n_{diss}(x, v) = -\gamma_n < v, n > n.$$

The tangential friction force is

$$F^t_{diss}(x, v) = -\gamma_t v^t = -\gamma_t < v, n^\perp > n^\perp$$

where

$$v^t = v - < v, n > n$$

is the tangential unit vector pointing into the direction of of the tangential component of the relative velocity and $n^\perp$ is the normal to n. R denotes the radius of pedestrians interactions, k_n is the interaction constant and γ_n, γ_t are suitable positive friction constants.

Remark 2.1. Finite size effects with a minimal radius around an individual pedestrian could be included using interaction potentials including a singularity. Other variants are given by an elliptical interaction force

$$f^n_{int}(x,v) = -\nabla_x V(x,v)$$

with a potential

$$V(x,v) = V(b(x,v))$$

consisting of

$$b(x,v) = \|x\| + \|x - vT_e\|$$

or by a force including the human vision cone.

2.1. **Optimal path.** Let ϕ be the travel costs for pedestrians to reach their destination. As one might expect, pedestrians intend to minimize these travel costs. Hughes [16, 17] proposed that pedestrians move in opposite to the gradient of the scalar potential ϕ, that is

$$d = -\frac{\nabla\phi}{\|\nabla\phi\|}. \tag{2.5}$$

The potential ϕ is determined by the nonlinear Eikonal equation

$$|\nabla\phi| = g(\rho) \text{ in } \Omega, \tag{2.6}$$

$$\phi = 0 \text{ on } \Omega_d \tag{2.7}$$

where Ω_d is the destination for pedestrians and $g(\rho)$ is a density-dependent cost function increasing in ρ. Pedestrians want to minimize the path length towards their destination but temper the estimated travel time by avoiding high densities. This behavior can be expressed by the 'density driven' rearrangement of the equipotential curves of ϕ using the cost function [16]

$$g(\rho) = \frac{1}{U(\rho)}.$$

3. Numerical Method

In this section, we present the numerical scheme we used in for simulations. The governing equations (2.1) are solved by a macroscopic particle method, see Ref. [30]. The particle method is based on a Lagrangian formulation of the hydrodynamic equations (2.1). We consider

$$\frac{dx}{dt} = u$$

$$\frac{d\rho}{dt} = -\rho\frac{\partial u}{\partial x}$$

$$\frac{du}{dt} = \hat{G}(\rho,\Phi,u) + \hat{F}(\rho,u).$$

One evaluates these quantities at the particle locations and approximates the spatial derivative of u by a difference approximation using a least square approach. In order to evaluate the interaction potential, the complete distance matrix $(d_{i,j}) = |x_i - x_j|$ has to be computed. Since this is costly, there is a restriction on the number particles which can be simulated in this way. In our case, we use an implementation with a nearest neighbor list reducing the computational effort considerably. The integral over the interaction potential is evaluated by a straightforward integration rule:

$$\hat{F}(\rho, u) \sim \sum_j F(x - x_j, u(x) - u_j)\rho_j dV_j$$

where dV_j is the local area around a particle determined by a nearest neighbor search. In case the numerical simulation is underresolved a higher order approximation of the integral has to be implemented. We refer to Ref. [21] for details. The resulting equations are then solved by a suitable time discretization. Diffusive terms can be included as well in a straightforward way using again a least squares approach to determine the finite difference approximation on the point cloud.

3.1. **Solving the Eikonal equation.** For our simulations, we use two types of grid points, one for solving the pedestrian flow model and another one for solving the Eikonal equation. Therefore, we establish two clusters of grid points, which are decoupled from each other, however, we interchange the necessary information from one cluster of grids to another and vice-versa. To update the velocity at each time step we need the gradient of the solution of the Eikonal equation to compute the direction vector (2.5). The Eikonal equation is a special case of the static Hamilton-Jacobi equation, for which many numerical methods have been developed, for example fast marching methods [19, 28], fast sweeping methods [35] or level set methods [26]. For complex geometries and non uniform problems, the fast marching method is quicker than the fast sweeping method [11]. But the disadvantage of the fast marching method is that it is applicable either to rectangular grids [28] or triangulation grids [19]. We use a mesh free method to solve the Eikonal equation which uses the idea of the fast marching method but differs in approximating the derivatives of the Eikonal equation. We use a least square approximation to approximate the derivatives. Our method has a time complexity of $O(N \log N)$ for N grid points. This corresponds to the complexity of the fast marching method but with the advantage that the mesh free approach can be used for any arbitrary point cloud.

3.2. **Boundary and Initial conditions.** For our simulations, we consider the following initial conditions for the density and velocity

$$\rho_0(x) = \begin{cases} \rho_0, & \text{if } x \in \Omega_0 \\ 0, & \text{otherwise} \end{cases}$$

and

$$u = 0 \tag{3.1}$$

where ρ_0 is a positive constant and Ω_0 describes a waiting area. The boundary condition for the Eikonal equation is

$$\begin{aligned} \phi(x) &= 0, \text{if } x \in \Omega_d \\ \phi(x) &= \infty, \text{if } x \in \Omega_w \end{aligned} \tag{3.2}$$

where Ω_d is the destination for pedestrians and Ω_w is the wall or obstacle in the domain.

3.3. Parameters.

We choose the desired speed and maximal density as in the experiments from [33, 34]. The free flow velocity is $1.55ms^{-1}$ and the maximum density is 3.7 pedestrians for m^2. Furthermore, we fix the time step size to $dt = 0.0001$ and set the relaxation parameter as $T = 0.001$. The interaction constant k_n is equal to 1000 and the friction and tangential coefficients are $\gamma_n = 10.0$ and $\gamma_t = 2.0$. The constants n_1 and n_2 in the speed-density relationship are set to 0.4 and 0.8 respectively.

4. Numerical Examples

In this section numerical results are presented. We are interested to reproduce the experimental results of pedestrian flows in straight corridor [33, 32] and through T-junctions [34], i.e. our numerical results are compared to the experimental data.

4.1. Example 1.

In the first example, we consider the uni-directional pedestrian flow in a straight corridor. The experimental set up from [32] is shown in Fig. 1.

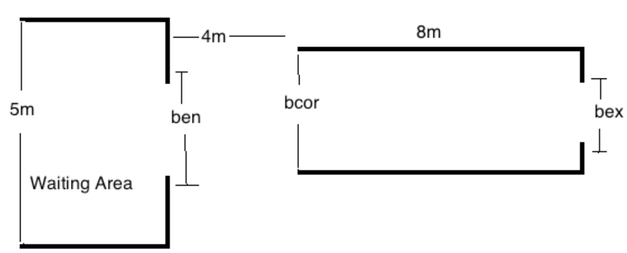

FIGURE 1. Straight corridor: sketch of the experimental setup where b_{cor} is the width of the corridor, b_{en} is the width of the entrance of the waiting area and b_{ex} is the width of the exit of the corridor.

The corridor is of length $8m$. Initially, participants stay in the waiting area. There is a $4m$ passage between the waiting area and the corridor to minimize the effect of b_{en}. In the experiments, the participants once they reach the exit of the corridor they will come back to the waiting area for another run. To emulate this behavior in our simulations, we provide the continuous stream of pedestrians. In Fig. 2, the trajectories of uni-directional pedestrian flow for high and low densities are shown. Fig.2(A) shows the trajectory of a uni-directional flow at high density and Fig. 2(B) shows the trajectory at low density. High density flow is obtained by $b_{en} > b_{ex}$ and low density flow is obtained by $b_{en} < b_{ex}$.

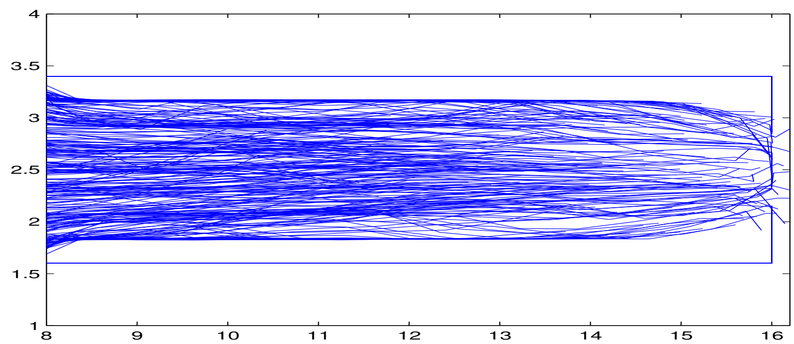

(A) High density: $b_{en} > b_{ex}$.

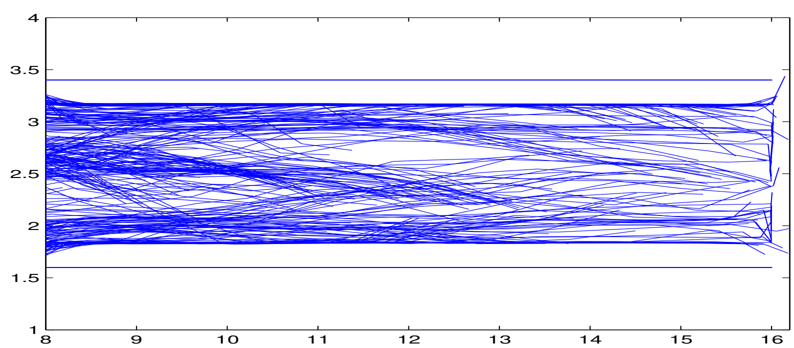

(B) Low density: $b_{en} < b_{ex}$.

FIGURE 2. Trajectories of pedestrians inside the corridor.

We investigate the influence of the corridor width on the fundamental diagram. Fig. 3 shows the relationship between density, velocity and flow for different sizes of corridor widths $b_{cor} = 1.8m$, $b_{cor} = 2.4m$ and $b_{cor} = 3.0m$. In Fig. 3 it can be observed that the width of the corridor has no effect on the fundamental diagram.

4.2. **Example 2.** In the second example, we consider the bi-directional pedestrian flow in a straight corridor. The experimental set up from [33] is shown in Fig. 4.

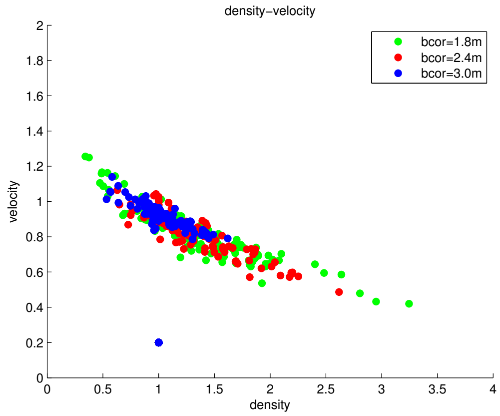

(A) Fundamental diagram: density vs. velocity.

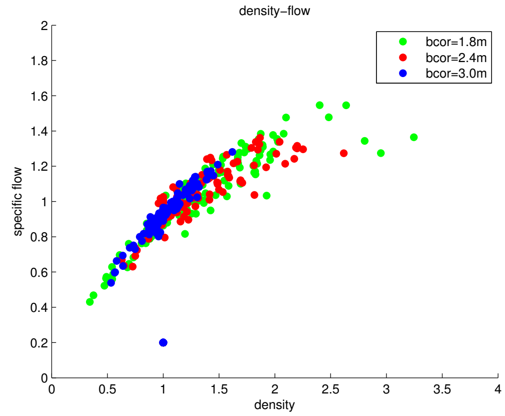

(B) Fundamental diagram: density vs. flow.

FIGURE 3. Comparison of fundamental diagrams for different corridor widths.

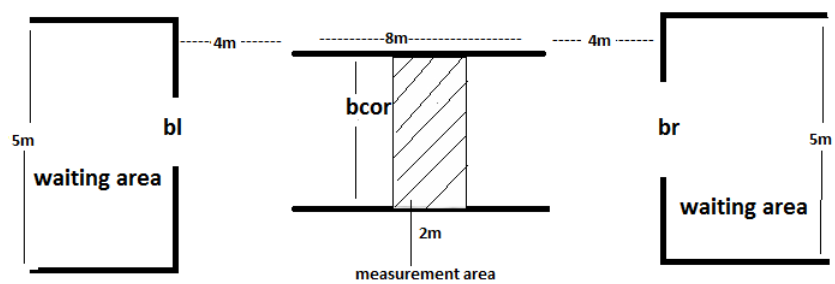

FIGURE 4. Straight corridor: sketch of the experimental setup where b_l and b_r are the width of the entrances of the waiting areas on the left and right side of the corridor.

The corridor is of length $8m$ and b_{cor} is the width of the corridor. Initially, pedestrians stand in the waiting areas stationed at both sides of the corridor. There is a $4m$ passage between the waiting area and the corridor to minimize the effect of b_l and b_r. In the experiments, when the participants arrive at the other side of the corridor, they leave the corridor and return to the waiting area for another run. In our simulations, we provide continuous stream of pedestrians in the waiting area to match with the experiments. To vary the form of the ordering, the participants get different instructions that result in different types of flows [33].

BFR-SSL flow: This type of flow is observed by using the same entrance width for both directions ($b_l = b_r$) and giving no instructions to the participants about which exit they have to choose.

BFR-DML flow: In this case also b_l is same as b_r, but the instruction to the participants is changed. The participants were asked to choose an exit at the end of the corridor according to a number given to them in advance.

UFR-DML flow: In this case the widths of entrances b_l and b_r are different and the participants are instructed to choose an exit at the end of the corridor according to a number given at the beginning.

In our simulations, to emulate the BFR-SSL flow, we solve the Eikonal equation two times with different boundary conditions. Since for the pedestrians in left waiting area, the destination is the right end of the corridor and for pedestrians in right waiting area, the left end of the corridor is the destination. We solve the Eikonal equation with right and left ends of the corridor as boundary conditions and the corresponding Eikonal solutions are ϕ_1 and ϕ_2 respectively. The velocity of left stream pedestrians is updated using ϕ_1 and the velocity of right stream pedestrians is updated using ϕ_2. Similarly, to emulate the BFR-DML and UFR-DML flows, we solve the Eikonal equation four times with right-bottom, right-top, left-bottom and left-top corners of the corridor as boundary conditions and ϕ_1, ϕ_2, ϕ_3 and ϕ_4 present the corresponding solutions of the Eikonal equations. The velocity of odd-numbered left stream pedestrians will be updated by using ϕ_1, even-numbered left stream pedestrians will be updated using ϕ_2. The velocity of odd-numbered right stream velocity is updated by using ϕ_3 and finally the velocity of even-numbered right stream pedestrians is updated by using ϕ_4. In Fig. 5, the trajectories of all these three flows are presented.

Lane formation: Lane formation is an important phenomenon in bi-directional flow. In Fig. 5, lane formation of pedestrians can be seen. In case of SSL flow, the pedestrians form two separate lanes and in case of DML flows, pedestrians form multiple lanes. In Figure 6, we plot the velocity profiles of BFR-DML flow for $b_{cor} = 3.6m$ and $b_l = b_r = 1.6m$ at $t = 13sec$ and $t = 51sec$. We calculate the density in classical way. Our density profiles match with the experimental results [33].

Fundamental diagram: For the analysis of fundamental diagrams, a rectangle with a length of $2m$ is chosen, see Fig. 4. To determine the fundamental diagram, we use the data from stationary flow. First, the influence of the corridor width on the fundamental diagram is studied. We consider $b_{cor} = 3.6m$ and $b_{cor} = 3.0m$ as two different widths of the corridor. Figure 7 shows the relationship between the density versus velocity and density versus specific flows. It can observed that the fundamental diagrams provide good results compared to the experimental data.

To investigate the influence of head-on conflicts and cross-directional conflicts in DML types of flow, numerical comparisons between the fundamental diagrams of SSL and DML flow for $b_{cor} = 3.6m$ are performed. The comparisons are presented in Fig. 8 and obviously both are consistent with each other. This means, head-on conflicts in multilanes have the same influence on the fundamental diagram as conflicts at the borders in stable separated lane flow. Due to limited computational time resources, the fundamental diagram is computed only for density values less than $2.0m^{-2}$ in the experiments for $b_{cor} = 3.0$.

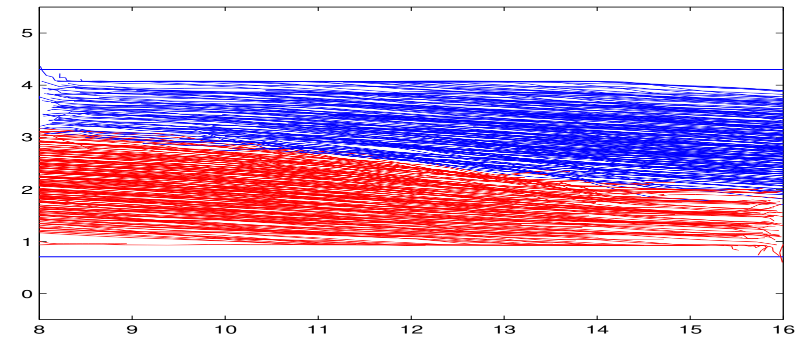

(A) BFR-SSL flow.

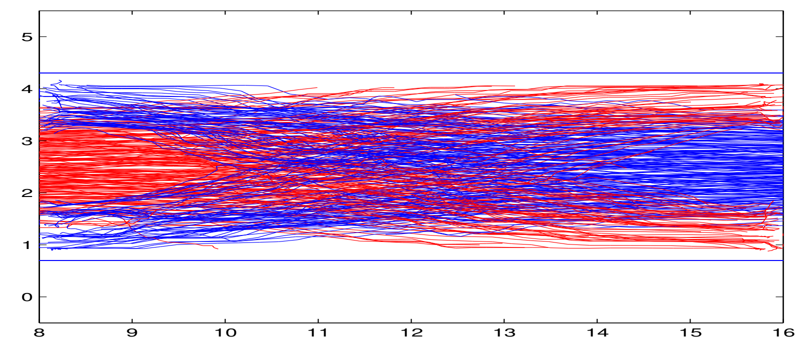

(B) BFR-DML flow.

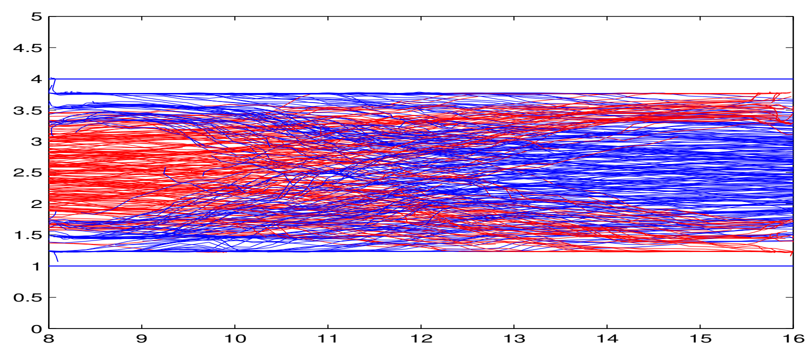

(C) UFR-DML flow.

FIGURE 5. Trajectories of pedestrians inside the corridor.

Finally, the influence of flow ratio of opposing streams on the fundamental diagram is studied. We compare the fundamental diagrams of BFR and UFR flow in Figure 9. It can be seen that the asymmetry in the flows does not affect the fundamental diagrams. In all three cases, our numerical results are consistent with the experimental data.

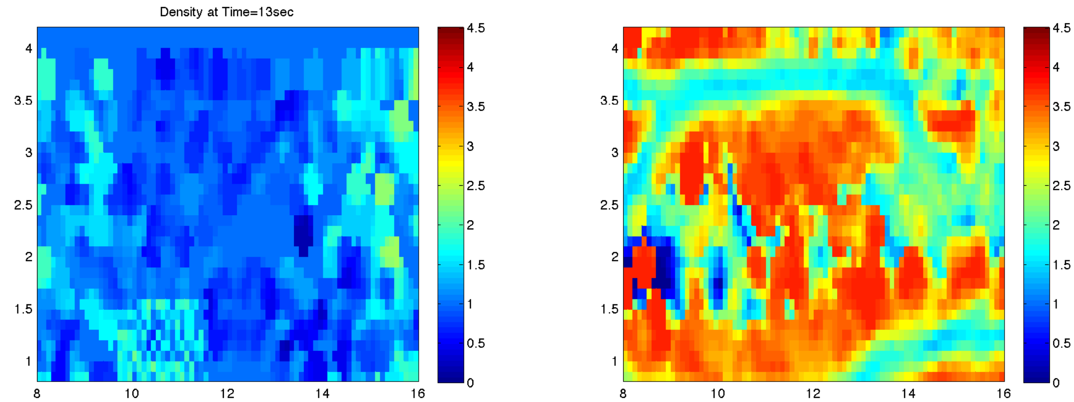

(A) Density at $t = 13sec$.

(B) Density at $t = 51sec$.

FIGURE 6. Density profiles at time $t = 13$ and $t = 51$ seconds.

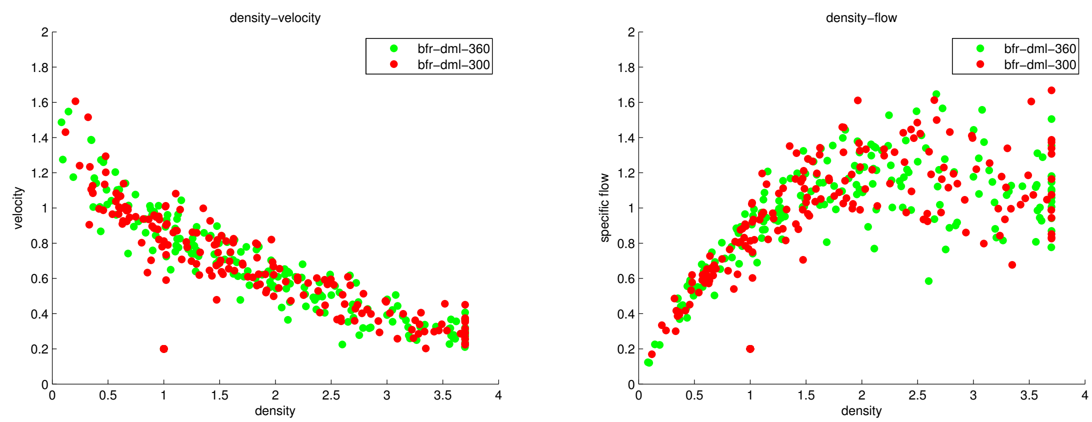

(A) Fundamental diagram: density vs. velocity.

(B) Fundamental diagram: density vs. flow.

FIGURE 7. Comparison of fundamental diagrams of DML flow for different corridor widths.

4.3. **Example 3:** In the third example, the pedestrian flow through a T-junction is considered. The experimental set up for the T-junction [34] is shown in Fig. 10.

Initially, the pedestrians are located in the waiting areas stationed at the left and right sides of the T-junction. Pedestrians move from two branches oppositely and then merge into the main stream at the T-junction. Here, b_{cor1} is the width of the corridor where pedestrians enter and b_{cor2} is the width of the corridor where pedestrians exit the T-junction, as shown in Fig. 10. To emulate the experiments, we provide the continuous pedestrian streams from both directions. As in the corridor example, there is a $4m$ passage between the T-junction and the waiting areas to minimize the effect of entrance. In this way, the flow in the corridor was nearly homogeneous over its entire width. Fig. 11 shows the pedestrian trajectories through the T-junction.

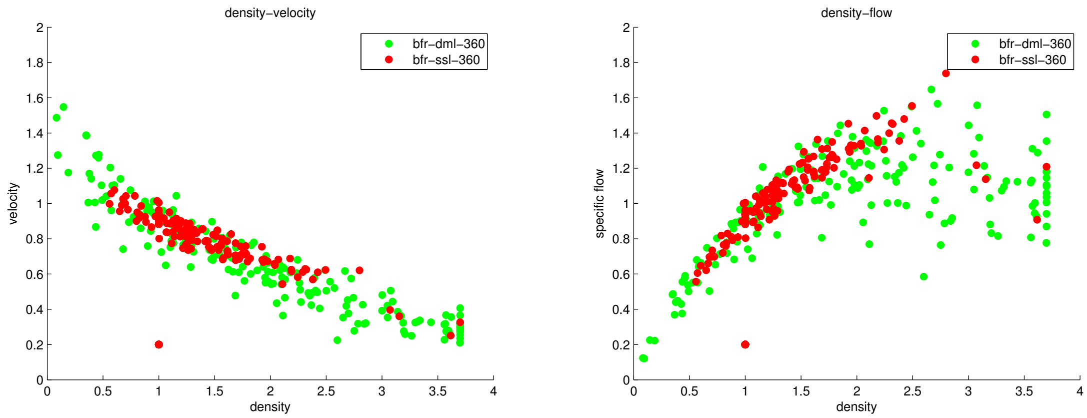

(A) Fundamental diagram: density vs. velocity. (B) Fundamental diagram: density vs. flow.

FIGURE 8. Comparison of fundamental diagrams for SSL and DML flow.

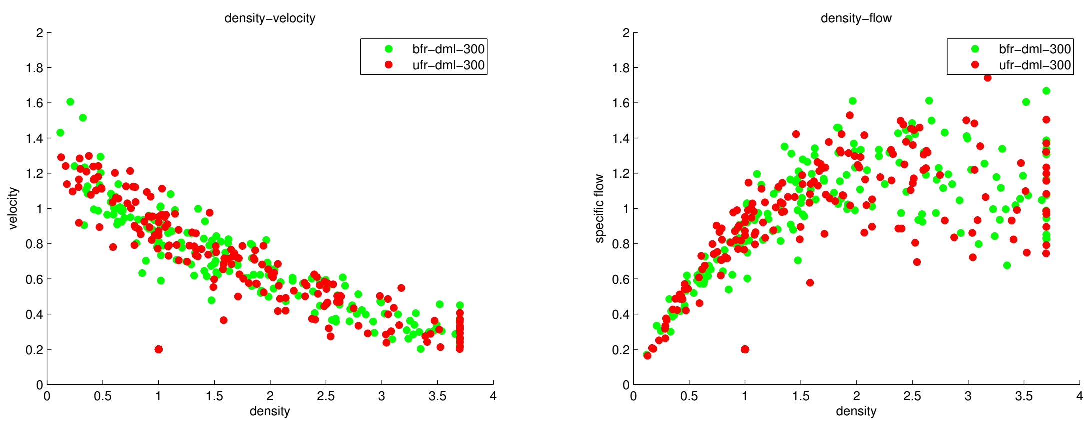

(A) Fundamental diagram: density vs. velocity. (B) Fundamental diagram: density vs. flow.

FIGURE 9. Comparison of fundamental diagrams for BFR and UFR flow.

In Fig 12, density profiles for low density and high density situations are presented. Density of the flow is varied by changing the width of the entrance of the waiting areas. For low density flow situation, the widths of the waiting area are set as $b_{en} = 2.4m$ and for high density flow situation, the widths of the waiting area are set as $b_{en} = 0.5m$. The density distribution in T-junction is not homogeneous both for low and high density situations. For low density situation, the higher density region locates at the main stream after merging and for the high density situation, high density region locates at junction. In Fig. 13, we compare the fundamental diagrams. The data assigned with 'T-left' and 'T-right' are measured in the areas before the streams merge, while the data assigned with 'T-front' are measured in the region where the streams have already merged. The locations of these measurements can be seen in the Fig. 10. In the experimental results by [34], the velocities of the

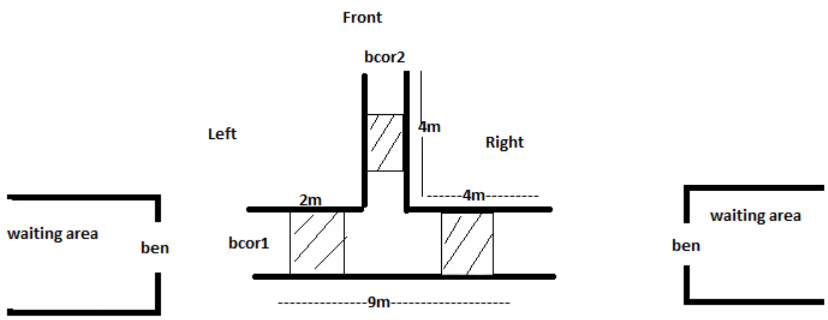

FIGURE 10. T-junction: sketch of the experimental setup where b_{en} is the width of the entrances of waiting areas at the left and right sides of the T-junction.

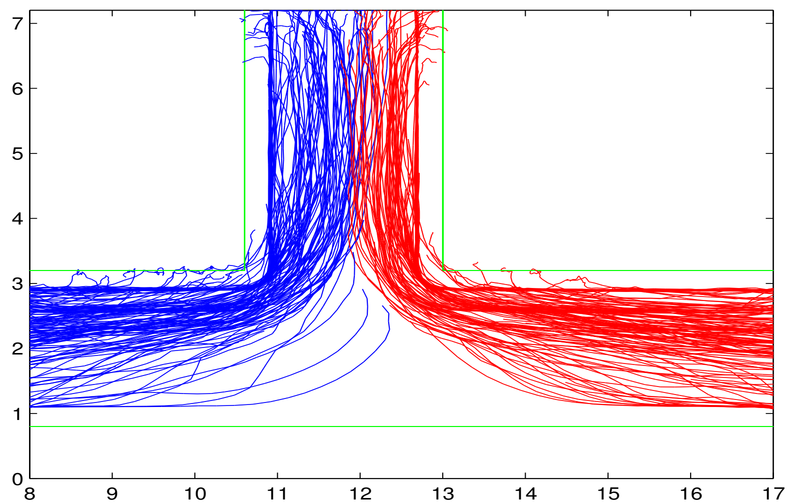

FIGURE 11. Trajectory of pedestrians through a T-junction.

pedestrians after merging is higher than the velocities of pedestrian before merging. This is because, before the merging pedestrians slow down near the corner when approaching pedestrians from the opposite stream. Another reason might be the fact that, when the destination is visible, pedestrians tend to walk fast. In our model, this idea is not included and can be considered as future work.

5. **Concluding Remarks**

We have presented a second order macroscopic model for the pedestrian flow where the desired direction is associated with the non-linear Eikonal equation. We have used a finite pointset method for solving the governing equations and the Eikonal equation. We have considered different test cases and compared our results with

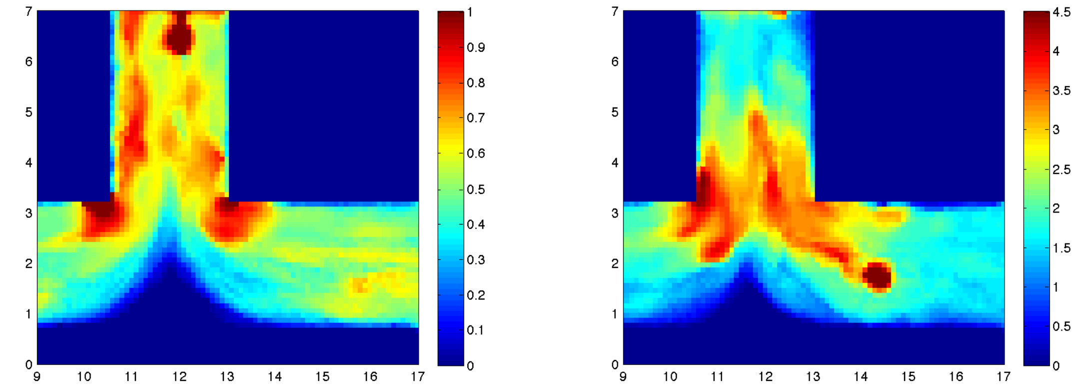

(A) low density profile (B) high density profile

FIGURE 12. Density profiles for low and high density situations.

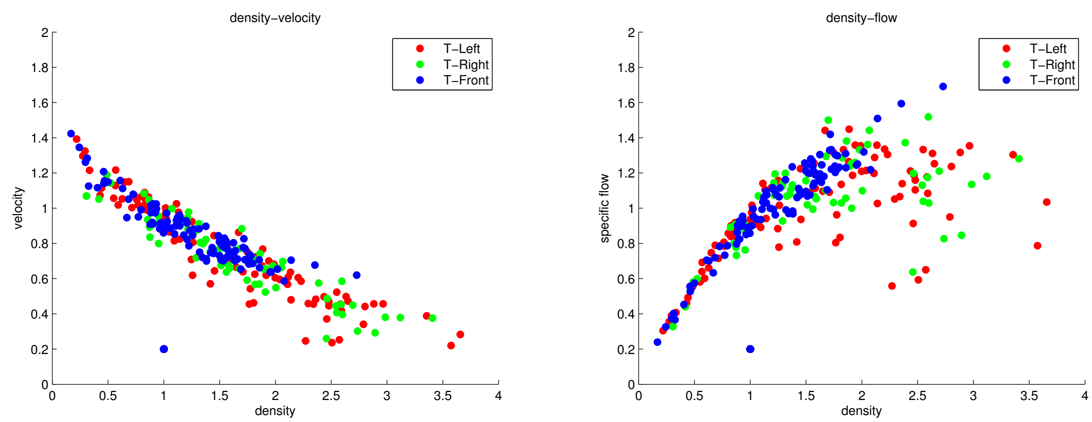

(A) Fundamental diagram: density vs. velocity. (B) Fundamental diagram: density vs. flow.

FIGURE 13. Fundamental diagrams of pedestrian flow at different measurement locations at a T-junction.

experimental data. In case of the T-junction, the slowing down of the velocity near the corner will be considered as future work.

Acknowledgements

This work is supported by the German research foundation, DFG grant KL 1105/20-1, by the Stiftung Rheinland-Pfalz für Innovation, Project EvaC, FKZ 989 and by the DAAD PhD programme MIC.

REFERENCES

[1] D. Amadoria, M. Di Francesco, The one-dimensional Hughes model for pedestrian flow: Riemann-type solutions, *Acta Mathematica Scientia*, 32:259–280, 2012.

[2] N. Bellomo, C. Dogbe, On the Modelling of Traffic and Crowds: A Survey of Models, *Speculations, and Perspectives*, Siam Review 53:409–463, 2011.

[3] N. Bellomo, C. Dogbe, On the modelling crowd dynamics from scaling to hyperbolic macroscopic models, *Math. Models Methods Appl. Sci.*, 18:1317–1345, 2008.

[4] J.A. Carrillo, A. Klar, S. Martin, S. Tiwari, Self-propelled interacting particle systems with roosting force, *Math. Mod. Meth. Appl. Sci.*, 20:1533–1552, 2010.

[5] J.A. Carrillo, M.R. D'Orsogna, V. Panferov, Double milling in self-propelled swarms from kinetic theory, *Kinetic and Related Models*, 2:363–378, 2009.

[6] R. Colombo, M. Garavello, M. Lecureux-Mercier, A Class of Non-Local Models for Pedestrian Traffic, *Math. Mod. Meth. Appl. Sci.*, 22:1150023, 2012.

[7] R. Colombo, M.D. Rosini, Pedestrian flows and non-classical shocks, *Math. Methods Appl. Sci.*, 28:1553–1567, 2005.

[8] P. Degond, C. Appert-Rolland, M. Moussaid, J. Pettre, G. Theraulaz, A hierarchy of heuristic-based models of crowd dynamics, *J. Stat. Phys.*, 152:1033–1068, 2013.

[9] C. Dogbe, On the modelling of crowd dynamics by generalized kinetic models, *J. Math. Anal. Appl.*, 387:512–532, 2012.

[10] R. Etikyala, S. Göttlich, A. Klar, S. Tiwari, Particle methods for pedestrian flow models: from microscopic to non-local continuum models, Math. Models Methods, Appl. Sci. DOI: 10.1142/S0218202514500274 (2014), accepted for publications.

[11] P.A. Gremaud and C.M. Kuster, Computational study of fast methods for the Eikonal equations, *SIAM J. Sci. Comp.*, 27:1803–1816, 2006.

[12] D. Helbing, Traffic and related self-driven many-particle systems, *Rev. Modern Phys.*, 73:1067–1141, 2001.

[13] D. Helbing, A fluid dynamic model for the movement of pedestrians, *Complex Systems*, 6:391–415, 1992.

[14] D. Helbing, I.J. Farkas, P. Molnar, T. Vicsek, Simulation of pedestrian crowds in normal and evacuation situations, in: M. Schreckenberg, S.D. Sharma (Eds.), Pedestrian and Evacuation Dynamics, Springer-Verlag, Berlin, pp. 21-58, 2002.

[15] D. Helbing and P. Molnar, Social force model for pedestrian dynamics, *Phys. Rev. E*, 51:4282–4286, 1995.

[16] R.L. Hughes, A continuum theory for the flow of pedestrians, *Transp. Res. Part B: Methodological*, 36:507–535, 2002.

[17] R.L. Hughes, The flow of human crowds, *Annu. Rev. Fluid Mech.*, 35:169–182, 2003.

[18] Y.Q. Jiang, R.X. Liu, Y.L. Duan, Numerical simulation of pedestrian flow past a circular obstruction, *Acta Mech. Sin.*, 27:215–221, 2011.

[19] R. Kimmel, J.A. Sethian, Fast marching method on Triangulated domains, *Proc. Nat'l Academy of Sciences*, 95:8341–8435, 1998.

[20] A. Klar, R.D. Kuhne, R. Wegener, Mathematical models for vehicular traffic, *Surv. Math. Ind.*, 6:215–239, 1996.

[21] A. Klar, S. Tiwari, A multi-scale meshfree particle method for macroscopic mean field interacting particle models, SIAM MMS 2014.

[22] C.D. Levermore, Relating Eddington factors to flux limiters, *J. Quant. Spectrosc. Radiat. Transf.*, 31:149–160, 1984.

[23] H. Ling, S.C. Wong, M. Zhang, C.H. Shu, W.H.K. Lam, Revisiting Hughes dynamic continuum model for pedestrian flow and the development of an efficient solution algorithm, *Transp. Res. Part B: Methodological*, 43:127-141, 2009.

[24] B. Maury, A. Roudneff-Chupin, F. Santambrogio, A macroscopic crowd motion model of the gradient-flow type, *Math. Mod. Meth. Appl. Sci.*, 20:1787–1821, 2010.

[25] H. Neunzert, The Vlasov equation as a limit of Hamiltonian classical mechanical systems of interacting particles, *Trans. Fluid Dynamics*, 18:663–678, 1977.

[26] S.J. Osher, R. Fedkew, Levelset methods and dynamic implicit surface, Springer, 2003.

[27] B. Piccoli, A. Tosin, Pedestrian flows in bounded domains with obstacles, *Contin. Mech. Thermodyn.*, 21:85–107, 2009.

[28] J.A. Sethian, Fast Marching Methods, *SIAM Review*, 41:199–235, 1999.

[29] H. Spohn, Large scale dynamics of interacting particles, Texts and Monographs in Physics, Springer, 1991.

[30] S. Tiwari, J. Kuhnert, Modelling of two-phase flow with surface tension by Finite Point-set method (FPM), *J. Comp. Appl. Math.*, 203:376–386, 2007.

[31] A. Treuille, S. Cooper, Z. Popovic, Continuum crowds, in: ACM Transaction on Graphics, *Proceedings of SCM SIGGRAPH*, 25:1160–1168, 2006.

[32] J. Zhang, W. Klingsch, A. Schadschneider, A. Seyfried, Transitions in pedestrian fundamental diagrams of straight corridors and T-junctions, *J. Stat. Mech.*, P06004, 2011.

[33] J. Zhang, W. Klingsch, A. Schadschneider, A. Seyfried, Ordering in bidirectional pedestrian flows and its influence on the fundamental diagram, *J. Stat. Mech*, 02002, 2012.

[34] J. Zhang, W. Klingsch, A. Schadschneider, A. Seyfried, Experimental study of pedestrian flow through a T-junction, Traffic and Granular Flow '11, 241–249, 2013.

[35] H. Zhao, A Fast sweeping method for Eikonal equation, *J. Math and Computing*, 74:603–627, 2005.